RSC Advances

PAPER

View Article Online
View Journal | View Issue

Cite this: *RSC Adv.*, 2023, **13**, 12703

The proton conduction behavior of two 1D open-framework metal phosphates with similar crystal structures and different hydrogen bond networks†

Kai-ming Zhang,[ac] Min-fang Ji,[b] Xue-Yi Zhou,[b] Fang Xuan,[b] Bo-yuan Duan,[a] Yuan Yuan,[a] Guang-xiang Liu,*[b] Hai-bao Duan*[b] and Hai-rong Zhao*[b]

Two open-framework zinc phosphates $[C_3N_2H_{12}][Zn(HPO_4)_2]$ (**1**) and $[C_6N_4H_{22}]_{0.5}[Zn(HPO_4)_2]$ (**2**) were synthesized *via* hydrothermal reaction and characterized by powder X-ray diffraction, thermogravimetric analysis and scanning electron microscopy. Both compounds have a similar crystal structure and macroscopic morphology. However, the difference in equilibrium cations, in which the propylene diamine is for **1** and the triethylenetetramine is for **2**, results in a significant distinction in the dense hydrogen grid. The diprotonated propylene diamine molecule in **1** is more favorable for forming a hydrogen-bond network in three dimensions than in **2**, in which the twisted triethylenetetramine forms a hydrogen bond grid with the inorganic framework only in two dimensions owing to its large steric effect. This distinction further leads to a disparity in the proton conductivity of both compounds. The proton conductivity of **1** can reach 1.00×10^{-3} S cm^{-1} under ambient conditions (303 K and 75% RH) and then increase to 1.11×10^{-2} S cm^{-1} at 333 K and 99% RH, which is the highest value among the open-framework metal phosphate proton conductors operated in the same conduction. In contrast, the proton conductivity of **2** is four orders of magnitude smaller than **1** at 303 K and 75% RH and two orders smaller than **1** at 333 K and 99% RH.

Received 20th February 2023
Accepted 20th March 2023

DOI: 10.1039/d3ra01130e

rsc.li/rsc-advances

1. Introduction

Crystallized porous materials, such as coordination polymers, metal–organic frameworks (MOFs) and covalent–organic frameworks (COFs), which are considered to be new candidates for proton conduction materials because of their high surface area, tunable pore surface and designable framework, have been attracting considerable attention owing to their potential applications in electrochemical devices, such as fuel cells,[1–7] sensing devices[8,9] and super capacitors.

Open-framework metal phosphates, composed of the anionic inorganic phosphate framework, which is formed by the metal ion and PO_4^{3-}, HPO_4^{2-}, $H_2PO_4^-$ or their complex substance, and organic amines or ammonium cations, are distinctive crystallize porous materials. They have similar designable structures to MOFs but have better thermal and aqueous stability owing to their robust inorganic units. Importantly, compared with MOFs, balanced organic amine cations (for example NH_4^+, enH_2^{2+}, $C_3N_2H_{12}^{2+}$ and Him^+) and the hydrophilic groups PO_4H/PO_4H_2 can directly provide an effective proton for proton transport. Moreover, the crystallinity of metal phosphates allows for the precise identification of their structural features to provide useful insights into proton-conduction pathways and mechanisms. Interestingly, most reported open-framework metal phosphates exhibit high proton conductivity. Yu reported JU103 (ref. 10) and JU102 (ref. 11) with the values of 3.59×10^{-3} S cm^{-1} (20 °C, 98% RH) and 1.19×10^{-3} S cm^{-1} (55 °C and 98% RH), respectively; Ren reported that compound $(C_2N_2H_{10})_{0.5}CoPO_4$ reached 2.05×10^{-3} S cm^{-1} (56 °C, 98% RH).[12] Our group has also carried out several studies on the preparation of highly conductive metal phosphates, such as $(C_2H_{10}N_2)[Mn_2(HPO_4)_3](H_2O)$ reached 1.64×10^{-3} S cm^{-1} at 298 K and 99% RH,[13] $(C_2H_{10}N_2)[Mn_2(PO_4)_2]\cdot 2H_2O$ reached 0.22×10^{-4} S cm^{-1} at 303 K and 99% RH (ref. 14) and $(NH_3(CH_2)_3NH_3)_2[Fe_4(OH)_3(HPO_4)_2(PO_4)_3]\cdot 4H_2O$[15] reached 0.8×10^{-3} S cm^{-1} at 317 K and 99% RH.

However, owing to the required balance of positive and negative charges in open-framework metal phosphate, its structural framework is fixed, which leads to its difficulty in increasing the proton conductivity by further modifying its structure using effective strategies, such as MOFs.[16–24] For example (1) inclusion of functional guest molecules into the cavity of MOFs, such as acid molecules, imidazoles, and triazoles;[25–31] (2) use of organic linkers bearing hydrophilic groups (including –COOH, –OH, $–SO_3H$, and $–PO_3H_2$)[32–38] as

[a]Department of Material Science and Engineering, Nanjing Institute of Technology, Nanjing 211167, P. R. China
[b]School of Environmental Science, Nanjing Xiaozhuang University, Nanjing 210009, P. R. China. E-mail: hairong_zhao111@163.com; Tel: +86 25 13914700426
[c]Jiangsu Key Laboratory of Advanced Structural Materials and Application Technology, 1 Hongjing Road, Nanjing 211167, P. R. China

† Electronic supplementary information (ESI) available. See DOI: https://doi.org/10.1039/d3ra01130e

structural building units. Therefore, the most ways to improve the proton conductivity of open-framework metal phosphate are by optimizing the conductive environment at present, for example, increasing the temperature and relative humidity and changing the water to an ammonia environment. Compared to the regulation of the material's structure, these changes in the external environment are not the fundamental and optimal way to improve proton conductivity. Therefore, to increase the proton conductivity of open-framework metal phosphate, the reasonable design of its original structure based on a thorough understanding of its proton transport mechanism is particularly important and critical. However, research in this area is still very poorly explored.

Moreover, open-framework metal phosphates or other crystallize porous materials generally exhibit excellent conductive behavior when high temperatures and high humidity coexist. However, it is also very important for proton-conducting materials to exhibit high proton conductivity in the medium-low temperature and humidity regions to maintain high conductivity over a wide temperature and humidity range, while research on high-proton conductive materials under relatively medium-low temperature and low humidity is still relatively lacking.[28,35,39–42]

Herein, to further understand the proton conduction mechanism of open-framework metal phosphates and to prepare materials that can exhibit high conductivity even at medium-low temperature and low humidity, we synthesized two metal phosphate compounds $[C_3N_2H_{12}][Zn(HPO_4)_2]$ (**1**) and $[C_6N_4H_{22}]_{0.5}[Zn(HPO_4)_2]$ (**2**) with similar crystal structures, both showing 1D ladder-like chain structure of the inorganic skeleton and the organic cations interspersed in the inorganic chains. The results demonstrate that the effective hydrogen bond grid plays a key role in proton transport. For **2**, the twisted structure of the large organic cationic triethylenetetramine resulted in the formation of hydrogen bond fragments only in the two-dimensional plane owing to its large steric hindrance, whereas **1** formed dense hydrogen bond interactions in the three-dimensional space. As anticipated, the value of proton conductivity for **1** reached 1.00×10^{-3} S cm^{-1} at low 75% RH and 303 K and then achieved 10^{-2} S cm^{-1} at 99% RH and 333 K, compared to the Nafion membrane; while for **2**, only 1.04×10^{-7} S cm^{-1} at low 75% RH and 298 K. To the best of our knowledge, **1** serves as the highest proton conductivity at low humidity in porous phosphate compounds. This encouraging result offers more opportunities for real-world conductive materials in fuel cells. It gives us more confidence to further investigate the relationship between proton conductivity and hydrogen bond network and organic amine cations to find a class of metal phosphate compounds that exhibit high electrical conductivity at low humidity.

2. Experimental section

2.1 Chemicals and reagents

All reagents and chemicals were purchased from commercial sources and used without further purification. Compounds **1** and **2** were synthesized according to the method reported in the literature.[43,44] The detailed preparation process is as follows.

2.2 Synthesis of $[C_3N_2H_{12}][Zn(HPO_4)_2]$ (1)

0.5480 g $Zn(ac)_2 \cdot 2H_2O$ was dispersed in 4.5 mL H_2O, 0.22 mL hydrochloric acid (35%) and 0.81 mL phosphoric acid (aq, 85 wt%). 1.26 mL of DAP was dropwise added to the mixture, which was homogenized for 30 min. The mixture solution was transferred and sealed in a 25 mL Parr Teflon lined stainless steel autoclave and heated at 438 K for 24 hours. The white plate crystals of **1** were obtained.

2.3 Synthesis of $[C_6N_4H_{22}]_{0.5}[Zn(HPO_4)_2]$ (2)

0.3255 g zinc oxide was dispersed in 7.2 mL H_2O, 0.7 mL hydrochloric acid (35%) and 2.6978 g phosphoric acid (aq, 85 wt%). 1.19 mL of TETA was dropwise added to the mixture, which was homogenized for 30 min. The mixture solution was transferred and sealed in a 25 mL Parr Teflon lined stainless steel autoclave and heated at 353 K for 50 hours. The white plate crystals of **2** were obtained.

2.4 Material characterizations

Powder X-ray diffraction (PXRD) data were collected using a Bruker D8 diffractometer with Cu Kα radiation ($\lambda = 1.5418$ Å) in the degree range of 5–50° (298 K). TGA experiments were performed using a STA449 F3 thermogravimetric analyzer in the temperature range of 298–1073 K (25–800 °C) at a warming rate of 10 °C min^{-1} under a nitrogen atmosphere, and the polycrystalline samples were placed in an Al_2O_3 crucible. The morphologies of the sample were observed using a Hitachi SU8010 scanning electron microscope (SEM).

2.5 Conductivity measurements

The hydrated proton conductivities of the compound pellets and composite membranes were measured using a CHI 660D electrochemical workstation and a conventional three-electrode method. The ac frequencies ranged from 10^2 to 10^6 Hz with 5 mV signal amplitude. The powdered polycrystalline pellets (with 0.7 mm thickness and 1.33 cm^2 area) prepared under 10 MPa pressure were sandwiched by two copper electrodes used for proton conductivity measurement. The conductivity (σ) of the sample was calculated using the following equation: $\sigma = L/RS$, where L and S represent the thickness and cross-sectional area of the sample, respectively, and R represents the resistance value obtained from the impedance spectra.

3. Results and discussion

The crystal structures of compounds **1** and **2** were first described, and then some differences between their structures were analyzed in detail to gain insight into conductive behavior. Compound **1** crystallized in the orthorhombic space group $P2_12_12_1$. Its asymmetric unit contains one Zn^{2+} ion (labeled Zn(1)), two crystallographically independent HPO_4^{2-} ions (labeled P(1) and P(2)), and one protonated diction of 1,3-

diaminopropane. As shown in Fig. 1, the Zn^{2+} showed tetrahedral coordination by four oxygen atoms, which all come from HPO_4^{2-} ions. The ZnO_4 and $HP(2)O_4$ were connected into four-membered rings, and then these four-membered rings were arranged around the *a* axis, forming a ladder-like chain. Moreover, the $HP(1)O_4$ tetrahedra are grafted onto the one-dimensional chain, which acts as a pendant. The action amine molecule, diprotonated DAP molecule, sits in the middle of these channels and interacts with the framework through hydrogen bonds.

Compound **2** crystallized in the monoclinic space group $P2_1/c$; its asymmetric unit is similar to that of **1**, which also contains one Zn^{2+} ion, two crystallographically independent HPO_4^{2-} ions and one quadruply protonated triethylenetetramine. As shown in Fig. 2, the Zn^{2+} ions of compound **2** have similar coordination structures to **1**, and then the ZnO_4 and $HP(2)O_4$ tetrahedra were also connected into a one-dimensional ladder-like chain, in which the quadruply triethylenetetramine molecule sits in the middle of these channels and interacts with the framework through hydrogen bonds.

Obviously, both compounds have a similar asymmetric unit and stacking structure. However, there is a great difference in the dense hydrogen bonds between the two compounds. As shown in Fig. 3(a), the nitrogen atom of the DAP with the oxygen of the phosphate has intense O···N distances for compound **1**, such as $d_{O8\cdots N1} = 2.965$ Å, $d_{O6\cdots N1} = 2.938$ Å, $d_{O5\cdots N1} = 2.818$ Å, $d_{O5\cdots N2} = 2.853$ Å, $d_{O7\cdots N2} = 2.881$ Å, and $d_{O4\cdots N2} = 2.966$ Å. These close distances extend in three dimensions, resulting in a dense hydrogen grid between the inorganic framework and the organic cations. Fig. 3(b) shows that the nitrogen atom of the triethylenetetramine with the oxygen of the phosphate has closer O···N distances, such as $d_{O8\cdots N1} = 2.891$ Å, $d_{O5\cdots N1} = 2.645$ Å, $d_{O5\cdots N2} = 2.681$ Å, and $d_{O6\cdots N2} = 2.688$ Å. Unfortunately, the twisted triethylenetetramine formed a hydrogen bond grid with the inorganic framework only in the ac plane owing to its large steric effect.

The experiment PXRD and FTIR of **1** and **2** are shown in Fig. 4 and S3,† respectively. The PXRD curves are consistent with those of the simulations, indicating that they have high purity (Fig. 4). Scanning electron microscopy (SEM) characterized the morphology of the obtained samples (Fig. 5) and demonstrated that the two compounds show a regular rod-like structure with similar diameter and length, which further indicates that they not only have a similar crystal structure but also have the same macroscopic morphology. As shown in Fig. S2,† the TG curves of compounds **1** and **2** showed similar one-step decomposition

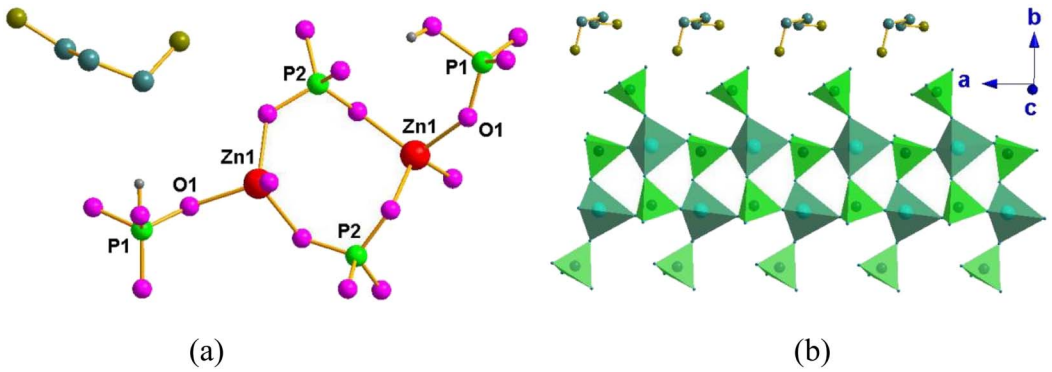

Fig. 1 (a) The asymmetric unit of **1** and (b) polyhedral view of **1** along the [100] axis showing a one-dimensional chain. The amine molecules are packed along the chains.

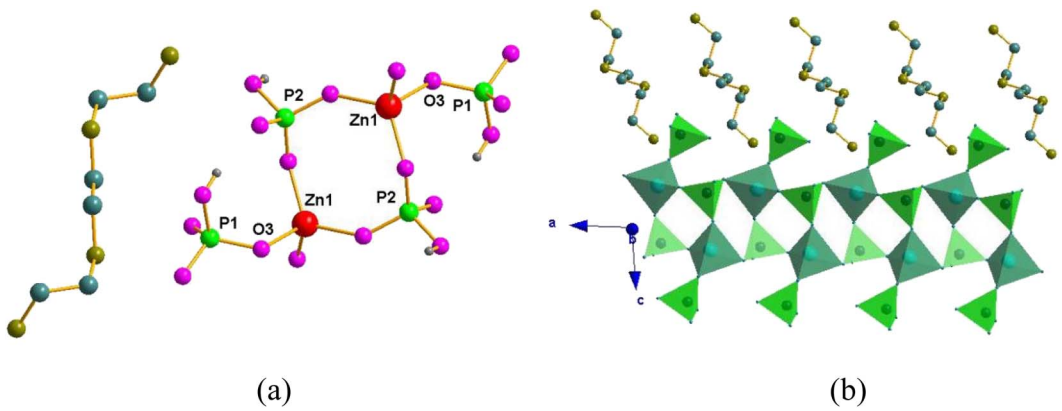

Fig. 2 (a) The asymmetric unit of **2** and (b) polyhedral view of **2** along the [100] axis showing a one-dimensional chain. The amine molecules are packed along the chains.

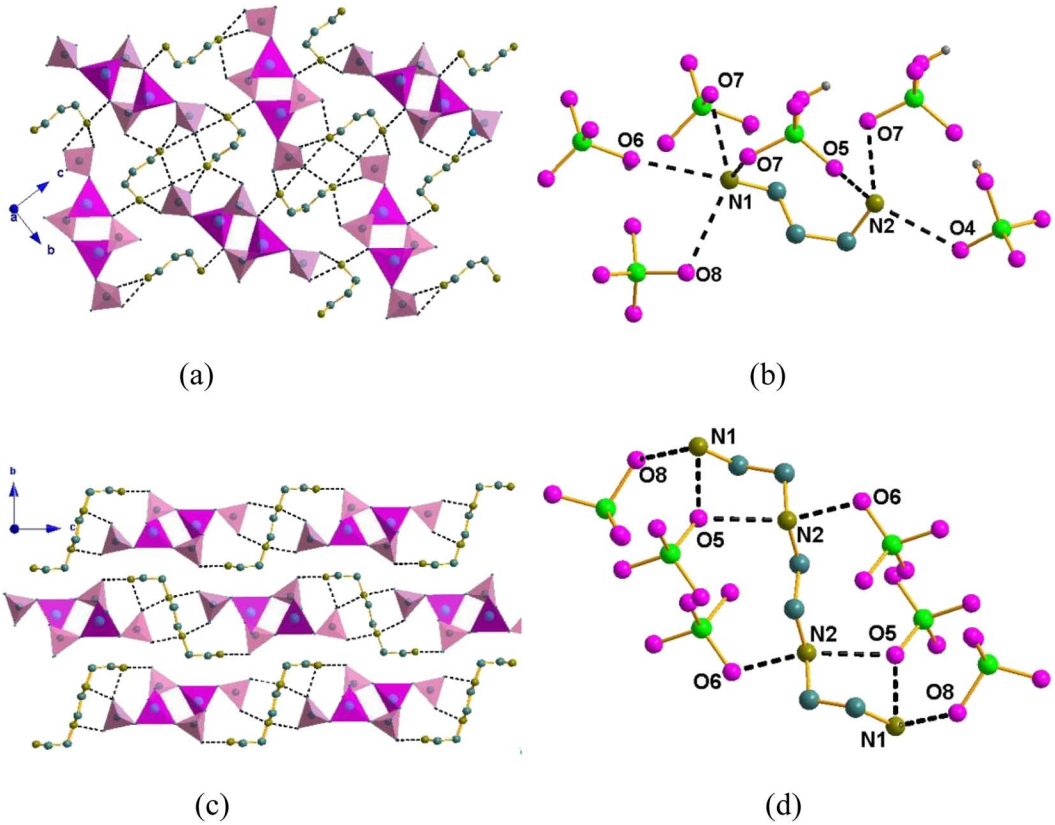

Fig. 3 H-bond interactions between the guests and the inorganic $[Zn(HPO_4)_2]_\infty$ chains in the crystals of (a) and (b) **1** and (c) and (d) **2**.

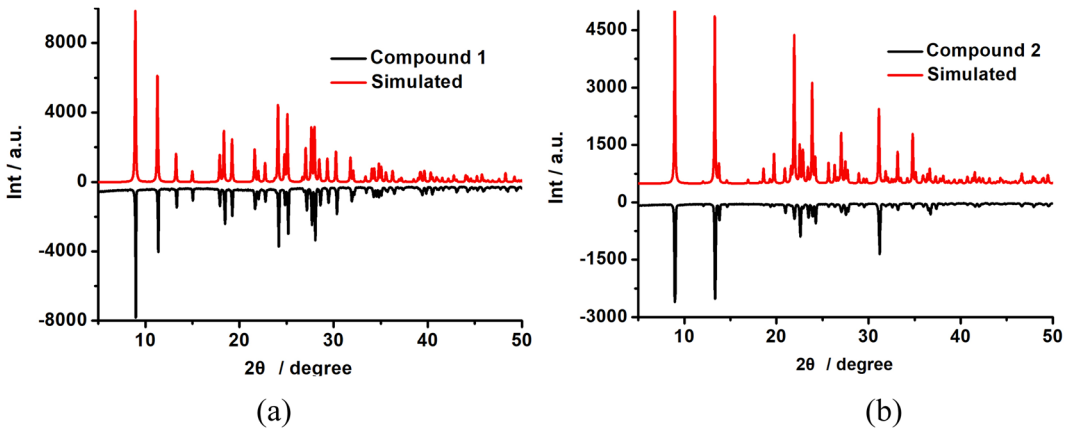

Fig. 4 PXRD patterns of (a) **1** and (b) **2** for the simulated and synthesized compounds.

thermogravimetric behavior. They started weight loss at 500 K and 527 K for **1** and **2**, respectively, which corresponded to the decomposition of charge-compensating cations occupied within the inorganic chains. The mass loss (*ca.* 29.5% and 29.3%) is also close to the calculated value (29.6%). The TG results demonstrated that **1** and **2** were thermally stable below *ca.* 500 K.

The conducting performance of the samples was first measured at a fixed temperature of 303 K with a humidity range of 75–99% RH using ac impedance spectroscopy. The unregular arc in the high frequency was observed corresponding to the boundary resistance and a spike in the low-frequency range related to the electrode contribution, respectively. As shown in Fig. S4,† both **1** and **2** have strong humidity-dependent proton conductivity; specifically, proton conductivity increases with humidity. Of the two compounds, compound **1** exhibited higher proton conductivity at low humidity. Its proton conductivity reached 1.00×10^{-3} S cm^{-1} at 75% RH, which is higher than almost all reported open-framework metal phosphates, such as $[HIm]_2[Zn_3(HPO_3)_4]$[28] (2.2×10^{-4} S cm^{-1}, 77% RH and 298 K),

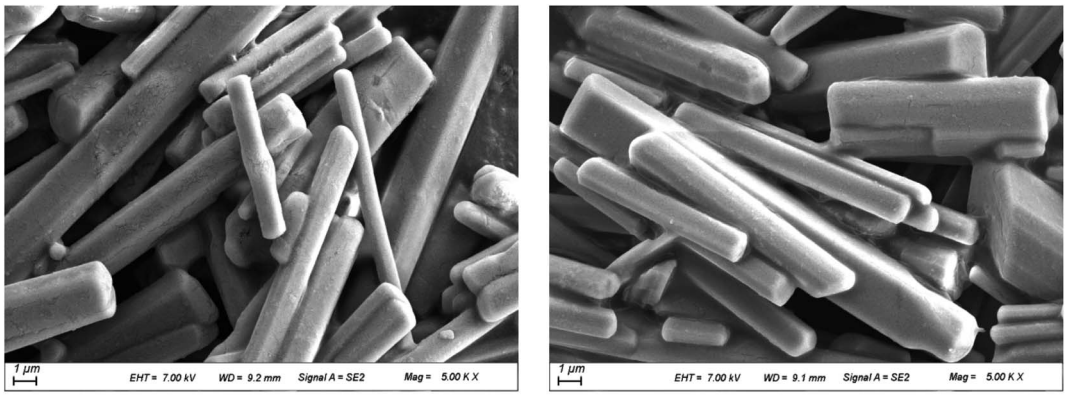

Fig. 5 SEM images of (a) compound **1** and (b) compound **2**.

which is also superior to most other types of crystallize porous materials, such as $(Me_2NH_2)_2(H_3O)[GdL_2]\cdot 8H_2O$[35] ($2.35 \times 10^{-4}$ S cm^{-1}, 60% RH and 298 K) and $\{R_3N(CH_2CO_2H)\}[MCr(ox)_3]\cdot nH_2O$[41] ($8 \times 10^{-5}$ S cm^{-1}, 60% RH and 298 K). Then, the values increased to 2.54×10^{-3} S cm^{-1} at 85% RH and achieved a maximum value of 8.33×10^{-3} S cm^{-1} at 99% RH.

However, for **2**, its proton conductivity is only 1.04×10^{-7} S cm^{-1} at 75% RH and then reaches 2.87×10^{-6} S cm^{-1} at 85% RH and 1.96×10^{-4} S cm^{-1} at 99% RH. In contrast, the proton conductivity of **2** is far less than that of **1** under the same conditions, but the gap narrowed with increasing humidity, which is four orders of magnitude difference at 75% RH and two orders of magnitude difference, while the proton conductivity increases to 99% RH. This indicates that the effective hydrogen bonding network between the proton-hoping sites (–HPO_4) and DAP for **1** is favorable for proton conduction under a low humidity environment by analyzing the structure of both compounds. The increasing proton conductivity with humidity of **1** and **2** shows that water molecules also play a role in proton conduction, which promotes effective proton transport because water molecules form proton carriers in the form of H_2O–H_3O^+ for proton hopping.

To gain insight into the influence of the structure of the compounds on proton conduction, we measured the water sorption isotherms of **1** and **2** at 298 K. The results show that the amount of water sorption for **1** is considerably higher than that for **2**, as shown in Fig. 6. This further indicates that a dense hydrogen bond grid in the chain is essential for the high conductivity of the compound.

Given the high proton conductivity of compound **1** at low RH, we further explored the variation in its proton conductivity with temperature under the same low RH condition. The temperature dependence of compound **1** was tested at fixed humidity of 75% RH, and the resultant curves in Fig. S5† show that the proton conductivity increased as the temperature increased. The values showed 1.00×10^{-3} S cm^{-1}, 1.32×10^{-3} S cm^{-1}, 1.64×10^{-3} S cm^{-1} and 1.97×10^{-3} S cm^{-1} at 303 K, 313 K, 323 K and 333 K, respectively. This indicates that compound **1** can exhibit high proton conductivity in a wide range of medium-low temperatures, and the extent of conductivity change is not large, which is conducive for stable proton transport in its practical application. Furthermore, we measured the temperature dependence of proton conductivity at 85% RH and 99% RH (Fig. 7 and S5†). At 85% RH, the values showed 2.54×10^{-3} S cm^{-1}, 2.99×10^{-3} S cm^{-1}, 3.21×10^{-3} S cm^{-1} and 3.43×10^{-3} S cm^{-1} at 303 K, 313 K, 323 K and 333 K, respectively; then, at 99% RH, the conductivity increased from 6.99×10^{-3} S cm^{-1} to 9.66×10^{-3} S cm^{-1} and reached the highest value of 1.11×10^{-2} S cm^{-1} at 333 K. This remarkable proton conduction of **1** (1.11×10^{-2} S cm^{-1}) is comparable to Nafion as well as several of the highest performing metal phosphate materials under the same conditions.

Similarly, it can also be clearly observed that the temperature dependence on the proton conductivity of compound **2** is proportional to the increasing temperature. The conductivity increased from 1.74×10^{-4} S cm^{-1} (298 K) to 2.82×10^{-4} S cm^{-1} (313 K) and reached 4.60×10^{-4} S cm^{-1} at 333 K and 99% RH. Undoubtedly, the value of **2** at any temperature point is lower than **1**.

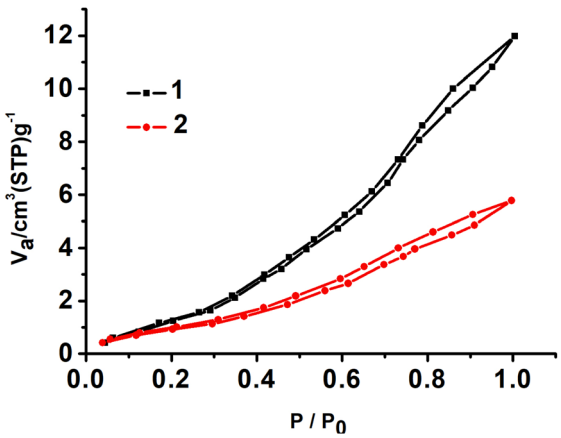

Fig. 6 Water-adsorption/desorption isotherm of **1** and **2** at 298 K.

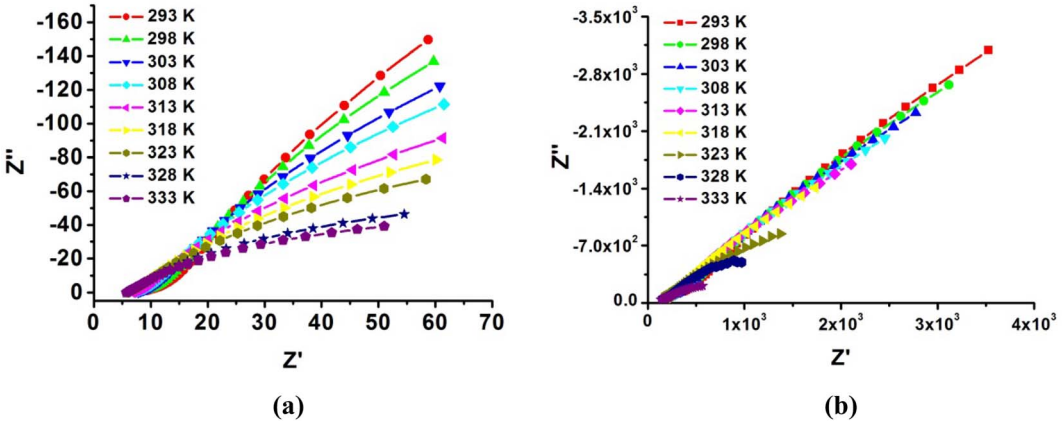

Fig. 7 Temperature-dependent of Nyquist plots of (a) compound **1** and (b) compound **2** at 99% RH.

To investigate the proton transfer mechanism, the activation energy (E_a) of **1** and **2** were obtained from the Arrhenius equation in the temperature range of 293–333 K:

$$\ln(\sigma T) = \ln A - \frac{E_a}{k_B T} \quad (1)$$

It can be induced that the activation energy is 0.24 eV (75% RH), 0.15 eV (85% RH) and 0.14 eV (99% RH) for **1**, demonstrating that **1** followed the Grothuss mechanism (Fig. 8 and S6†). The activation energy of **2** is 0.23 eV at 99% RH, indicating that the proton transfer mechanism of **2** also belongs to the Grothuss mechanism at this conduction. The calculated activation energy, together with the structural difference between both compounds, is helpful in obtaining insight into the proton pathways. For **1**, the three-dimensional hydrogen bond network can absorb more water molecules to construct intense hydrogen bond networks in the chains for proton hopping, resulting in a lower E_a and Grotthuss mechanism in proton conduction. However, at high RH, **2** can also absorb more water molecules into the inter-chain spaces; therefore, **2** preferred to form efficient proton-hopping pathways rather than the migration of the cations owing to its large hindrance, resulting in the Grotthuss mechanism.

These results demonstrate that the intense hydrogen bond networks play an important role in the proton conducting of open-framework metal phosphates and that the appropriate size of the organic amine cations helps to form denser hydrogen bonds. For example, the diprotonated DAP molecules in **1** are more favorable for forming a dense hydrogen-bond network in three dimensions than in compound **2**, in which the twisted triethylenetetramine formed a hydrogen bond grid with the inorganic framework only in two dimensions owing to its large steric effect. Compared with the previously prepared 1D compound $(C_4H_{12}N_2)_{1.5}[Fe_2(OH)(H_2PO_4)(HPO_4)_2(PO_4)]\cdot H_2O$ (**3**), its larger size piperazine leads to the formation of weaker hydrogen bonds, which also makes the proton conductivity of **3** (2.61×10^{-4} S cm^{-1} at 99% RH and 293 K) lower than **2**.

Moreover, in addition to organic equilibrium cations, we pay attention to the important role of inorganic frameworks in the construction of hydrogen bond grids of open-framework metal phosphates. For example, the two previously prepared 2D open-framework metal phosphates $(C_2H_{10}N_2)[Mn_2(HPO_4)_3(H_2O)]$ (**4**) and $(C_2H_{10}N_2)[Mn_2(PO_4)_2]\cdot 2H_2O$ (**5**) have the same organic equilibrium cations but various inorganic frameworks. The more hydrogen bonding sites of the inorganic framework in **4** resulted in proton conductivity (1.65×10^{-3} S cm^{-1}), which was

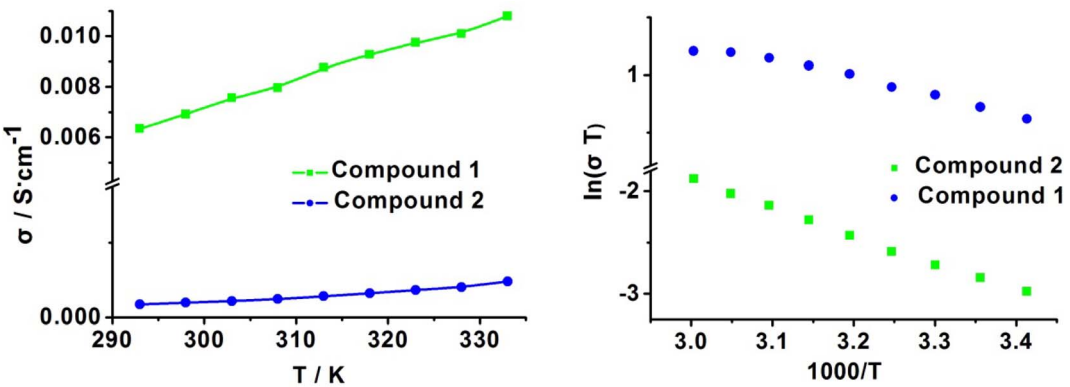

Fig. 8 The corresponding conductivity in the form of (a) σ *vs.* T and (b) ln(σT) *vs.* 1000/T at 99% RH for **1** and **2**.

much higher than **5** (1.14×10^{-5} S cm^{-1}) under the same conditions (293 K and 99% RH). Therefore, the design of an inorganic framework with abundant hydrogen bonding sites and matching suitable small molecular equilibrium cations can form dense hydrogen bonds, which is helpful for obtaining highly conductive open-framework metal phosphates. Further studies to design and prepare open-framework metal phosphates with high proton conductivity based on the above two aspects of analysis are in progress and will be reported in due course.

4. Conclusion

In summary, we fabricated two 1D zinc phosphates $[C_3N_2H_{12}][Zn(HPO_4)_2]$ (**1**) and $[C_6N_4H_{22}]_{0.5}[Zn(HPO_4)_2]$ (**2**) with similar crystal structures. For **1**, the pendant phosphoate groups of the inorganic framework and the 1,3-diaminopropane formed an intense hydrogen bond network for proton conducting, which exhibited high proton conductivity of 1.00×10^{-3} S cm^{-1} at 75% RH (303 K) and then up to 1.11×10^{-2} S cm^{-1} at 99% RH (333 K). For **2**, the pendant phosphoate groups and the triethylenetetramine formed only hydrogen bond fragments in the planes owing to the larger steric hindrance of cations, which gives the result that the values only reached 10^{-4} S cm^{-1} at 99% RH. These detailed investigations demonstrate that the suitable size of the organic cations in **1** is helpful for the formation of efficient hydrogen bond grids and then provide efficient proton-conductive pathways in a wide humidity range. This study provides the promise of selecting appropriate organic amine for constructing reasonable proton conducting pathways in metal phosphates to improve conductivity. Our group will further study the relationship between the structure of the compound and proton conductivity.

Conflicts of interest

There are no conflicts to declare.

Acknowledgements

The authors thank the Foundation of the Jiangsu Education Committee (20KJB150006), Major Project of Nanjing Institute of Technology Innovation Fund (CKJA202001) for financial support. The present work was supported by the outstanding scientific and technological innovation team in colleges and universities of Jiangsu province (202211276140H).

References

1 K.-D. Kreuer, S. J. Paddison, E. Spohr and M. Schuster, Transport in Proton Conductors for Fuel-Cell Applications: Simulations, Elementary Reactions, and Phenomenology, *Chem. Rev.*, 2004, **104**, 4637–4678.
2 B. C. H. Steele and A. Heinzel, Materials for Fuel-Cell Technologies, *Nature*, 2001, **414**, 345–352.
3 M. Inukai, S. Horike, T. Itakura, R. Shinozaki, N. Ogiwara, D. Umeyama, S. Nagarkar, Y. Nishiyama, M. Malon, A. Hayashi, T. Ohhara, R. Kiyanagi and S. Kitagawa, Encapsulating Mobile Proton Carriers into Structural Defects in Coordination Polymer Crystals: High Anhydrous Proton Conduction and Fuel Cell Application, *J. Am. Chem. Soc.*, 2016, **138**, 8505–8511.
4 G. Shen, J. Liu, H. B. Wu, P. Xu, F. Liu, C. Tongsh, K. Jiao, J. Li, M. Liu, M. Cai, J. P. Lemmon, G. Soloveichik, H. Li, J. Zhu and Y. Lu, Multi-functional anodes boost the transient power and durability of proton exchange membrane fuel cells, *Nat. Commun.*, 2020, **11**, 1191–1202.
5 H. W. Zhang and P. K. Shen, Recent Development of Polymer Electrolyte Membranes for Fuel Cells, *Chem. Rev.*, 2012, **112**, 2780–2832.
6 H. Yuan, H. F. Dai, X. Z. Wei and P. W. Ming, Model-based observers for internal states estimation and control of proton exchange membrane fuel cell system: A review, *J. Power Sources*, 2020, **468**, 228376.
7 J. Zhang, B. Hu, X. Deng, C. Li, Y. S. Wu, C. Zhou, D. Z. Zhang, L. Ge, W. Zhou and Z. P. Shao, Perovskite-Carbon Joint Substrate for Practical Application in Proton Exchange Membrane Fuel Cells under Low-Humidity/High-Temperature Conditions, *ACS Appl. Mater. Interfaces*, 2022, **14**, 30872–30880.
8 M. Dogru, M. Handloser, F. Auras, T. Kunz, D. Medina, A. Hartschuh, P. Knochel and T. Bein, A Photoconductive Thienothiophene-Based Covalent Organic Framework Showing Charge Transfer Towards Included Fullerene, *Angew. Chem.*, 2013, **52**, 2920–2924.
9 D. Gopalakrishnan and W. R. Dichtel, Direct Detection of RDX Vapor Using a Conjugated Polymer Network, *J. Am. Chem. Soc.*, 2013, **135**, 8357–8362.
10 Y. J. Sun, Y. Yan, Y. Y. Wang, Y. Li, J. Y. Li and J. H. Yu, High proton conduction in a new alkali metal-templated open-framework aluminophosphate, *Chem. Commun.*, 2015, **51**, 9317–9319.
11 Y. Mu, Y. Wang, Y. Li, J. Li and J. H. Yu, Organotemplate-free synthesis of an open-framework magnesium aluminophosphate with proton conduction properties, *Chem. Commun.*, 2015, **51**, 2149–2151.
12 M. Wang, H. B. Luo, S. X. Liu, Y. Zou, Z. F. Tian, L. Li, J. L. Liu and X. M. Ren, Water assisted high proton conductance in a highly thermally stable and superior water-stable open-framework cobalt phosphate, *Dalton Trans.*, 2016, **45**, 19466–19472.
13 H. R. Zhao, C. Xue, C. P. Li, K. M. Zhang, H. B. Luo, S. X. Liu and X. M. Ren, A Two-Dimensional Inorganic-Organic Hybrid Solid of Manganese(II) Hydrogenophosphate Showing High Proton Conductivity at Room Temperature, *Inorg. Chem.*, 2016, **55**, 8971–8975.
14 K. M. Zhang, F. Y. He, H. B. Duan and H. R. Zhao, An Alkali Metal Ion-Exchanged Metal-Phosphate $(C_2H_{10}N_2)_xNa_{1-x}[Mn_2(PO_4)_2]$ with High Proton Conductivity of 10^{-2} S·cm^{-1}, *Inorg. Chem.*, 2019, **58**, 6639–6646.
15 H. R. Zhao, Y. Jia, Y. Gu, F. Y. He, K. M. Zhang, Z. F. Tian and J. L. Liu, A 3D open-framework iron hydrogenophosphate showing high proton conductance under water and aqua-ammonia vapor, *RSC Adv.*, 2020, **10**, 9046–9051.

16 X. Chen and G. Li, Proton conductive Zr-based MOFs, *Inorg. Chem. Front.*, 2020, **7**, 3765–3784.
17 D. W. Lim and H. Kitagawa, Proton Transport in Metal-Organic Frameworks, *Chem. Rev.*, 2020, **120**, 8416–8467.
18 Y. X. Ye, L. S. Gong, S. C. Xiang, Z. J. Zhang and B. L. Chen, Metal-Organic Frameworks as a Versatile Platform for Proton Conductors, *Adv. Mater.*, 2020, **32**, 1907090.
19 P. Ramaswamy, N. E. Wong and G. K. H. Shimizu, Proton Conduction in Metal-Organic Frameworks and Related Modularly Built Porous Solids, *Chem. Soc. Rev.*, 2014, **43**, 5913–5932.
20 X. Y. Dong, J. H. Wang, S. S. Liu, Z. Han, Q. J. Tang, F. F. Li and S. Q. Zang, Synergy between Isomorphous Acid and Basic Metal-Organic Frameworks for Anhydrous Proton Conduction of Low-Cost Hybrid Membranes at High Temperatures, *ACS Appl. Mater. Interfaces*, 2018, **10**, 38209–38216.
21 S. Horike, D. Umeyama and S. Kitagawa, Ion Conductivity and Transport by Porous Coordination Polymers and Metal-Organic Frameworks, *Acc. Chem. Res.*, 2013, **46**, 2376–2384.
22 S. Chand, S. M. Elahi, A. Pal and C. D. Madhab, Metal Organic Frameworks and Other Crystalline Materials for Ultrahigh Superprotonic Conductivities of 10^{-2} $S{\cdot}cm^{-1}$ or Higher, *Chem. - Eur. J.*, 2019, **25**, 6259–6269.
23 X. Meng, H. N. Wang, S. Y. Song and H. J. Zhang, Proton-conducting crystalline porous materials, *Chem. Soc. Rev.*, 2017, **46**, 464–480.
24 A. L. Li, Q. Gao, J. Xu and X. H. Bu, Proton-conductive metalorganic frameworks: Recent advances and perspectives, *Coord. Chem. Rev.*, 2017, **344**, 54–82.
25 C. R. Kayaramkodath, I. Rajith, D. V. Sairam, P. Joseph, C. W. Vivek, K. V. R. Goudappagouda, K. Sreekumar and S. B. Sukumaran, Imidazole-Linked Crystalline Two-Dimensional Polymer with Ultrahigh Proton-Conductivity, *J. Am. Chem. Soc.*, 2019, **141**, 14950–14954.
26 F. M. Zhang, L. Z. Dong, J. S. Qin, W. Guan, J. Liu, S. L. Li, M. Lu, Y. Q. Lan, Z. M. Su and H. C. Zhou, Effect of Imidazole Arrangements on Proton-Conductivity in Metal-Organic Frameworks, *J. Am. Chem. Soc.*, 2017, **139**, 6183–6189.
27 Q. Qiao, H. J. Wang, C. P. Li, X. Z. Wang and X. M. Ren, Improving proton conduction of the Prussian blue analogue $Cu_3[Co(CN)_6]_2 \cdot nH_2O$ at low humidity by forming hydrogel composites, *Inorg. Chem. Front.*, 2021, **8**, 2305–2314.
28 R. Shankar, E. Jakhar, A. Dubey, P. Chauhan, P. K. Tiwari and S. Basu, Studies on the Genesis and Proton Conductivity of Imidazole-Based Linear and Open-Framework Zinc Phosphites, *Inorg. Chem.*, 2021, **60**, 6569–6575.
29 R. Li, S. H. Wang, X. X. Chen, J. Lu, Z. H. Fu, Y. Li, G. Xu, F. K. Zheng and G. C. Guo, Highly Anisotropic and Water Molecule-Dependent Proton Conductivity in a 2D Homochiral Copper(II) Metal-Organic Framework, *Chem. Mater.*, 2017, **29**, 2321–2331.
30 S. Bureekaew, S. Horike, M. Higuchi, M. Mizuno, T. Kawamura, D. Tanaka, N. Yanai and S. Kitagawa, One-Dimensional Imidazole Aggregate in Aluminium Porous Coordination Polymers with High Proton Conductivity, *Nat. Mater.*, 2009, **8**, 831–836.
31 S. Horike, D. Umeyama, M. Inukai, T. Itakura and S. Kitagawa, Coordination -Network-Based Ionic Plastic Crystal for Anhydrous Proton Conductivity, *J. Am. Chem. Soc.*, 2012, **134**, 7612–7615.
32 X. M. Li, Y. M. Wang, Y. Mu, J. Liu, L. Zeng and Y.-Q. Lan, Superprotonic Conductivity of a Functionalized Metal-Organic Framework at Ambient Conditions, *ACS Appl. Mater. Interface*, 2022, **14**, 9264–9271.
33 W. J. Phang, H. Jo, W. R. Lee, J. H. Song, K. Yoo, B. Kim and C. S. Hong, Superprotonic Conductivity of a UiO-66 Framework Functionalized with Sulfonic Acid Groups by Facile Postsynthetic Oxidation, *Angew. Chem., Int. Ed.*, 2015, **54**, 5142–5146.
34 Z. N. Que, Y. X. Ye, Y. S. Yang, F. H. Xiang, S. M. Chen, J. L. Huang, Y. B. Li, C. L. Liu, S. C. Xiang and Z. J. Zhang, Solvent-Assisted Modification to Enhance Proton Conductivity and Water Stability in Metal Phosphonates, *Inorg. Chem.*, 2020, **59**, 3518–3522.
35 S. L. Zhang, Y. X. Xie, M. R. Yang and D. R. Zhu, Porosity regulation of metal-organic frameworks for high proton conductivity by rational ligand design: mono-versus disulfonyl-4,4'-biphenyldicarboxylic acid, *Inorg. Chem. Front.*, 2022, **9**, 1134–1142.
36 B. G. Montse, R. S. Inés, M. P. C. Rosario, X. Konstantinos, V. Didier, S. Norbert, L. G. Mar, d. R. Carmen, R. L. Enrique, C. Aurelio, D. D. Konstantinos and O. P. Pascual, Layered Lanthanide Sulfophosphonates and Their Proton Conduction Properties in Membrane Electrode Assemblies, *Chem. Mater.*, 2019, **31**, 9625–9634.
37 P. Bhanja, A. Palui, S. Chatterjee, Y. V. Kaneti, J. Na, Y. Sugahara, A. Bhaumik and Y. Yamauchi, Crystalline Porous Organic Polymer Bearing $-SO_3H$ Functionality for High Proton Conductivity, *ACS Sustainable Chem. Eng.*, 2020, **8**, 2423–2432.
38 M. Subhabrata, D. Joyashish, S. Chandani, S. Rudraditya, O. Basu and S. K. Das, Designing UiO-66-Based Superprotonic Conductor with the Highest Metal-Organic Framework Based Proton Conductivity, *ACS Appl. Mater. Interfaces*, 2019, **11**, 13423–13432.
39 R. Wang, X. Y. Dong, H. Xu, R. B. Pei, M. L. Ma, S. Q. Zang, H. W. Hou and C. W. M. Thomas, Super water-stable europium-organic framework: guests inducing low humidity proton conduction and sensing of metal ions, *Chem. Commun.*, 2014, **50**, 9153–9156.
40 J. Z. Li, H. Wu, L. Cao, X. Y. He, B. B. Shi, Y. Li, M. Z. Xu and Z. Y. Jiang, Enhanced Proton Conductivity of Sulfonated Polysulfone Membranes under Low Humidity via the Incorporation of Multifunctional Graphene Oxide, *ACS Appl. Nano Mater.*, 2019, **2**, 4734–4743.
41 M. Sadakiyo, H. Ōkawa, A. Shigematsu, M. Ohba, T. Yamada and H. Kitagawa, Promotion of Low-Humidity Proton Conduction by Controlling Hydrophilicity in Layered Metal-Organic Frameworks, *J. Am. Chem. Soc.*, 2012, **134**, 5472–5475.

42 H. A. Patel, N. Mansor, S. Gadipelli, D. J. L. Brett and Z. X. Guo, Superacidity in Nafion/MOF Hybrid Membranes Retains Water at Low Humidity to Enhance Proton Conduction for Fuel Cells, *ACS Appl. Mater. Interface*, 2016, **8**, 30687–30691.

43 W. T. A. Harrison, Z. Bircsak, L. Hannooman and Z. H. Zhang, Two New 1,3-Diammonium-Propane Zinc Hydrogen Phosphates: $H_3N(CH_2)_3NH_3{\cdot}Zn_2(HPO_4)_2(H_2PO_4)_2$, with 12-Ring Layers, and $H_3N(CH_2)_3NH_3.Zn(HPO_4)_2$, with 4-Ring Ladders, *J. Solid State Chem.*, 1998, **136**, 93–102.

44 A. Choudhury, S. Neeraj, S. Natarajana and C. N. R. Rao, Transformations of the low-dimensional zinc phosphates to complex open-framework structures. Part 2:{one-dimensional ladder to two and three-dimensional structures, *J. Mater. Chem.*, 2001, **11**, 1537–1546.